DePaepe Gael (Orcid ID: 0000-0001-9701-3593)

On the use of radio-frequency offsets for improving double quantum homonuclear dipolar recoupling of half-integer quadrupolar nuclei

Nghia Tuan Duong[1,2,#], Daniel Lee[1,⊥], Frédéric Mentink-Vigier[1,$], Olivier Lafon[2,3]*, and Gaël De Paëpe[1]*

[1] Univ. Grenoble Alpes, CEA, IRIG-MEM, 38000 Grenoble, France.

[2] Univ. Lille, CNRS, Centrale Lille, Univ. Artois, UMR 8181 – UCCS – Unité de Catalyse et Chimie du Solide, F-59000 Lille, France.

[3] Institut Universitaire de France, Paris 75231, France.

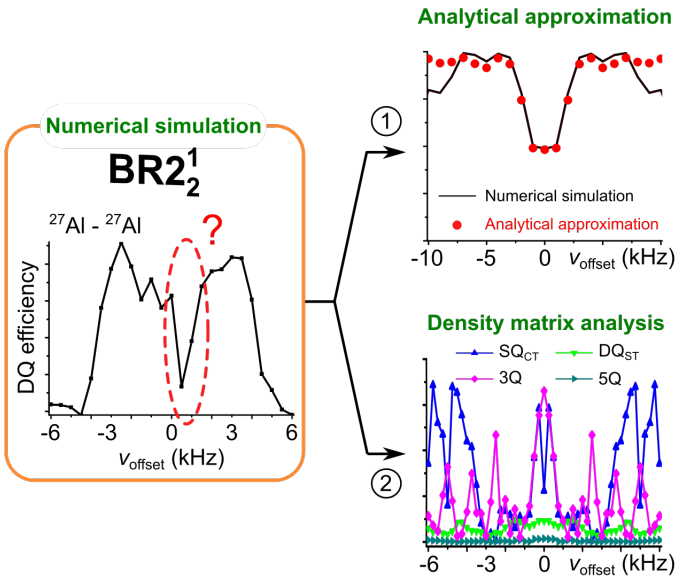

* Corresponding authors: Olivier Lafon (E-mail: olivier.lafon@univ-lille.fr), Gaël De Paëpe (E-mail: gael.depaepe@cea.fr)

Current affiliation:

[#] NMR Science and Development Division, RIKEN SPring-8 Center, and Nano-Crystallography Unit, RIKEN-JEOL Collaboration Center, Yokohama, Kanagawa 230-0045, Japan

This is the author manuscript accepted for publication and has undergone full peer review but has not been through the copyediting, typesetting, pagination and proofreading process, which may lead to differences between this version and the Version of Record. Please cite this article as doi: 10.1002/mrc.5142

[ǂ] Department of Chemical Engineering and Analytical Science, University of Manchester, Sackville Street, Manchester, M13 9PL, UK

[$] National High Magnetic Field Laboratory, Florida State University, 1800 E. Paul Dirac Dr, Tallahassee, 32301, FL, USA

Abstract

Detecting proximities between nuclei is crucial for atomic-scale structure determination with NMR spectroscopy. Different from spin-1/2 nuclei, the methodology for quadrupolar nuclei is limited for solids due to the complex spin dynamics under simultaneous magic-angle spinning (MAS) and radio-frequency irradiation. Herein, the performance of several HORROR-based homonuclear dipolar recoupling sequences are evaluated for ^{27}Al (spin-5/2). It is shown numerically and experimentally on mesoporous alumina that $BR2_2^1$ outperforms the supercycled S_3 sequence and its pure double quantum (DQ) (bracketed) version, [S_3], both in terms of DQ transfer efficiency and bandwidth. This result is surprising since the S_3 sequence is among the best low power recoupling schemes for spin-1/2. The superiority of $BR2_2^1$ is thoroughly explained and the crucial role of radio-frequency offsets during its spin dynamics is highlighted. The analytical approximation of $BR2_2^1$, derived in an offset-toggling frame, clarifies the interplay between offset and DQ efficiency, namely the benefits of off-resonance irradiation and the trough in DQ efficiency for $BR2_2^1$ when the irradiation is central between two resonances, both for spin-1/2 and half-integer-spin quadrupolar nuclei. Additionally, density matrix propagations show that the $BR2_2^1$ sequence, applied to quadrupolar nuclei with larger quadrupolar interactions, can create single- and multiple quantum coherences for near on-resonance irradiation. This significantly perturbs the creation of DQ coherences between central transitions of neighboring quadrupolar nuclei. This effect explains the DQ efficiency trough for near on-resonance irradiation, both in the case of cross and autocorrelation peaks. Overall, this work aids experimental acquisition of homonuclear dipolar correlation spectra of half-integer-spin quadrupolar nuclei and provides theoretical insights towards improving recoupling schemes at high magnetic field and fast MAS.

1. Introduction

Correlation spectroscopy utilizing the "through-space" dipolar interaction is important in nuclear magnetic resonance (NMR) since it facilitates spectral assignments and reveals internuclear spatial proximities. Such correlation information is achieved by the combined use of magic-angle spinning (MAS) [1] of the sample, for high-resolution solid-state NMR spectra through the averaging of anisotropic interactions (such as chemical shift anisotropy (CSA) and dipolar interaction), and the selective reintroduction of the dipolar interaction using radio-frequency (RF) pulses known as recoupling sequences [2–6].

Contrary to the well-developed homonuclear dipolar recoupling sequences for spin-1/2 nuclei, this area is much less explored for quadrupolar nuclei (spin $I > ½$). The primary obstacle for quadrupolar nuclei comes from the larger number of energy levels, equal to $2I+1$, and the additional presence of the quadrupolar interaction, which originates from the interaction of the intrinsic electric quadrupolar moment of a particular nucleus with spin $I > 1/2$ and the electric field gradient (EFG) that this nucleus experiences [7–11]. The magnitude of this interaction varies depending on the values of the two parameters mentioned above, and it can range from zero to tens of MHz. Moreover, the quadrupolar interaction is anisotropic and has a magnitude that usually greatly exceeds that of RF irradiation and MAS. In this case, the quadrupolar interaction leads to complicated spin dynamics under both the application of RF irradiation and MAS. Hence, initial homonuclear dipolar recoupling methods for quadrupolar nuclei avoided the utilization of RF-fields by using off-magic-angle spinning [12–14] or Rotational Resonance (R^2) [15]. The former recovers not only the homonuclear dipolar coupling but also other anisotropic interactions, such as the CSA and the first-order quadrupolar interaction. These unwanted interactions can severely broaden the spectra, making their interpretation difficult. The latter enables the dipolar recoupling of two nuclei when their chemical shift difference matches one- or two-times the MAS frequency. The application of R^2 is thus limited since it is only feasible at specific MAS frequencies and for specific pairs of nuclei.

A more versatile but complicated approach for homonuclear dipolar recoupling of quadrupolar nuclei involves the application of suitable RF irradiation under MAS conditions [16–20]. To partially alleviate the complex spin dynamics of half-integer-spin quadrupolar nuclei, a possible solution is to focus on the central transition (CT) between energy levels $m_I = -1/2$ and $+1/2$ with m_I the azimuthal quantum number since this transition is immune to the first-order quadrupolar interaction. Recoupling based on the selective irradiation of the CTs requires a weak RF-field in order to limit the excitation of satellite transitions (STs) and the related signal losses [21–23]. For instance, in order to spin-lock the transverse magnetization related to the CT of a spin-3/2 nucleus, the RF-field should be adjusted so that $0.1 < \kappa < 0.3$, where κ is defined as the ratio of the applied RF-field (ν_{RF}) and the MAS frequency (ν_R) [16]. Outside this range, the signal loss for the CT is significant. Such RF-field amplitude requirement for efficient CT spin-locking is compatible with the double-quantum (DQ) homonuclear rotary recoupling (HORROR) sequence [24], since it sets the CT nutation frequency (ν_{CT}) equal to half of ν_R, (i.e. $\nu_{CT} = (I+1/2)\nu_{RF} = \nu_R/2$, which can also be written $\nu_{RF}/\nu_R = \kappa = 1/(2I+1) = 0.25$ for $I = 3/2$ and 0.17 for $I = 5/2$). Indeed, several HORROR-based recoupling sequences have been introduced to excite the DQ coherences between CTs (DQ_{CT}) of half-integer-spin quadrupolar nuclei and were successfully applied for structural investigations of complex systems [18,25–27]. However, the achieved DQ efficiency is low compared to that for spin-1/2 nuclei because of (i) the larger size of density matrix for increasing I-spin value, since the density matrix of a pair of spin-I nuclei has a size equal to $(2I+1)^2\times(2I+1)^2 = 4\times4$, 16×16 and 36×36 for $I = 1/2$, 3/2 and 5/2, respectively, whereas the DQ coherences between $1/2\leftrightarrow-1/2$ transitions of these nuclei (i.e. the DQ_{CT} for $I > 1/2$) correspond only to two elements of the density matrix and (ii) the overlap between the various transitions of quadrupolar nuclei for a powder and the time dependence of the transition frequencies under MAS, which often prevents the selective irradiation of a given transition required for the efficient creation of DQ_{CT}. Hence, the DQ_{CT} efficiency decreases for higher I-spin quantum number. Another difficulty is that these sequences are highly sensitive to the carrier frequency owing to the required weak RF-field and the presence of chemical and quadrupolar induced shifts. This

clearly limits the application of these recoupling sequences to systems exhibiting small offset differences. This drawback is accordingly more severe for larger magnetic field strengths because the isotropic chemical shift differences also become larger. Thus, the quest for a robust and efficient homonuclear dipolar recoupling sequence for quadrupolar nuclei is not straightforward. For a further description of homonuclear dipolar recoupling sequences for half-integer-spin quadrupolar nuclei, the reader is referred to extensive reviews of Edén [28,29].

The symmetry-based pulse sequence $R2_2^1$ [30–32] belongs to the family of HORROR-based sequences. A supercycling of $R2_2^1$ with an introduction of a phase-reversal symmetry in the middle yields the sequence $BR2_2^1$, which has shown a notable robustness to large offsets and RF-field inhomogeneities for spin-1/2 nuclei [33–37] and for quadrupolar nuclei relative to other DQ homonuclear dipolar recoupling sequences [38]. However, $BR2_2^1$ is still offset-dependent, meaning that inappropriate placement of the carrier frequency (ν_{offset}) can prevent the observation of sites of interest [39]. Also founded on the RN_n^ν symmetry-based recoupling theory [32], Edén and coworkers introduced a new family of recoupling sequences conforming to the HORROR condition, denoted as S_p sequences, where p is an integer [40]. These well-designed sequences enable an efficient reintroduction of the homonuclear dipolar interaction with excellent compensation for offset as well as RF-field inhomogeneity, outperforming $BR2_2^1$ for ^{13}C-^{13}C systems [40]. Very recently, these S_p sequences have been applied to correlate the CTs of half-integer-spin quadrupolar nuclei in the single quantum – single quantum (SQ-SQ) manner [41,42].

In this work, we compare the performances of $BR2_2^1$ and S_3 recoupling sequences for DQ-SQ homonuclear correlation between ^{27}Al ($I = 5/2$) nuclei, and also further explore the underlying spin dynamics. Numerical and experimental evaluations are presented, and a comprehensive theoretical description is provided to explain the superiority of $BR2_2^1$ over other recoupling sequences in terms of DQ transfer efficiency and bandwidth. Notably, the key role of radio-frequency offsets during the $BR2_2^1$ spin dynamics is explained.

2. Pulse sequence

The standard notation for RF pulses is ξ_θ, indicating a rectangular RF pulse with flip angle ξ and phase θ. The flip angle is given in radians while the phase is in degrees. The $BR2_2^1$ recoupling sequence, shown in Fig. 1a, can be written as $(R2_2^1)_n(R2_2^{-1})_n$, in which $R2_2^1$ employs a simple $(\pi)_0$-pulse as a basic element and n is the number of loops. The duration of one cycle of $BR2_2^1$ is equal to $4\tau_R$, where τ_R is a rotor period and equals $1/\nu_R$. The family of S_p sequences can be written as $\left(R2_{2^p}^1 R2_{2^p}^{-1}\right)_n$. In our work, we use the sequence with $p = 3$, which has been shown to be highly efficient for spin-½ nuclei [40]. This S_3 sequence is displayed in Fig. 1b, in which the basic composite pulse employed is $R_3 = (2\pi)_{180}(3\pi/2)_0(\pi/2)_{180}$. One cycle of S_3 lasts for $16\tau_R$, which is four times longer than $BR2_2^1$ with n =1. The S_3 recoupling sequence can be bracketed by two π/2 pulses with phases of 180° and 0° to produce pure DQ recoupling and is denoted as [S_3] and depicted in Fig. 1c. Fig. 1d shows the pulse sequence used to record the ^{27}Al one-dimensional (1D) DQ-filtered spectra and its corresponding coherence transfer pathway. The first recoupling block (denoted as "DQ exc"), lasting for τ_{exc}, generates DQ coherences from the total longitudinal magnetization, proportional to the sum of the longitudinal spin angular momentum operators, I_{jz}. The subsequent CT-selective π pulse selects the DQ coherences between CT energy levels m_I = −1/2 and m_I = +1/2 of a pair of dipolar-coupled quadrupolar nuclei and removes the DQ coherences between energy levels m_I and m_I+2 of a single I-spin nucleus. Then the second recoupling block (denoted as "DQ rec"), whose duration is τ_{rec}, reconverts the DQ coherences into longitudinal magnetization, which is converted into SQ coherence by the CT-selective π/2 read-pulse. Here, we employed $\tau_{exc} = \tau_{rec}$ since this condition yields maximal transfer efficiency. The mixing time (τ_{mix}) is defined as the sum of τ_{exc} and τ_{rec}.

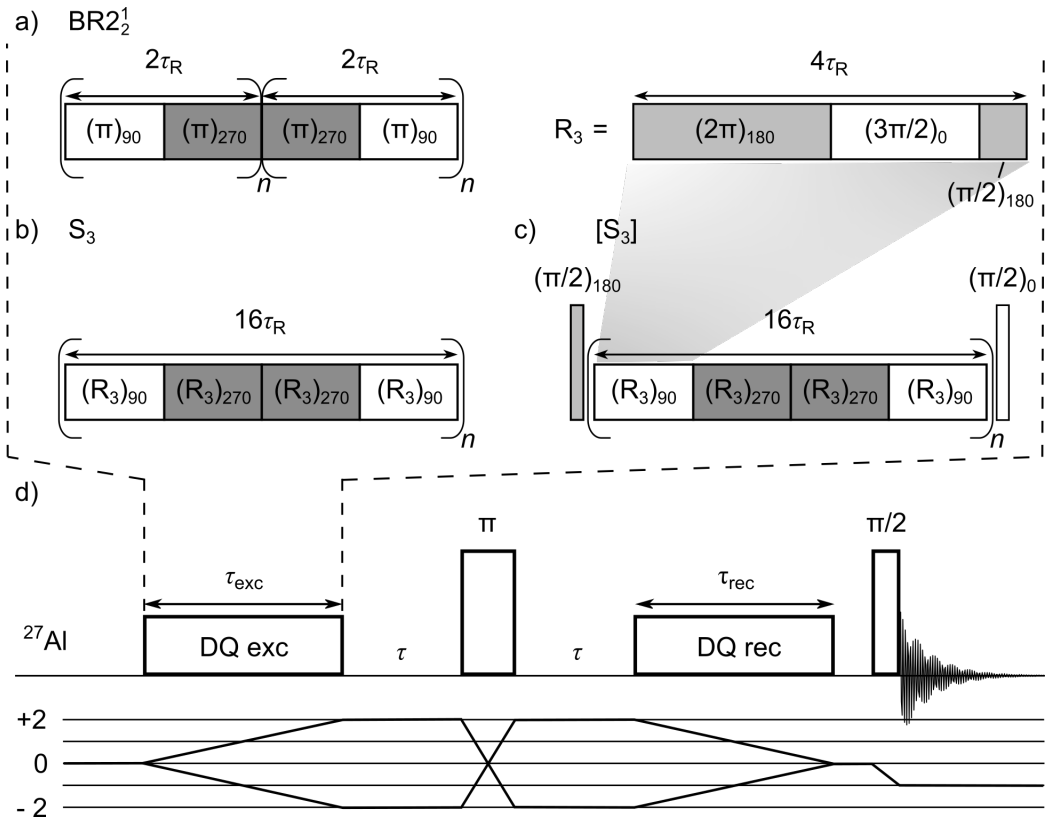

Figure 1. Homonuclear dipolar recoupling sequences: (a) $BR2_2^1$, (b) S_3, and (c) $[S_3]$, where *n* is the number of loops. The basic composite pulse R_3 for the creation of S_3 and $[S_3]$ is shown at the top right of the figure. (d) Pulse sequence (top) and coherence transfer pathway (bottom) of ^{27}Al DQ-filtered 1D experiment employing the homonuclear recoupling sequences of subfigures a, b, and c. All the RF pulses depicted in the figure are CT-selective. The coherence transfer pathway is selected using a 64-step nested phase cycle, for which the phases of the DQ excitation block, the central π pulse, and the reading pulse are incremented in 90°, 45°, and 180° steps, respectively [18]. The τ delays bracketing the central π pulse were equal to $(\tau_R-\tau_\pi)/2$ for $BR2_2^1$ and S_3 recoupling and $(\tau_R-\tau_\pi)/2-\tau_{\pi/2}$ for $[S_3]$, where $\tau_{\pi/2}$ and τ_π are the lengths of the π/2 bracketing pulses of $[S_3]$ recoupling and central π pulse, respectively.

3. DQ efficiency evaluation

3.1. Numerical simulations

Fig. 2 compares the simulated DQ efficiencies for $BR2^1_2$, S_3 and $[S_3]$ for a powder of ^{27}Al-^{27}Al spin pairs. The spin system consists of two ^{27}Al nuclei (Al_1 and Al_2) with a dipolar coupling $b_{12}/(2\pi) = -0.3$ kHz and no CSA. Both ^{27}Al nuclei were subject to quadrupolar interactions with a quadrupolar coupling constant $C_Q = 3.0$ MHz and an asymmetry parameter for the EFG tensor, $\eta_Q = 0.25$. The Euler angles relating the internuclear ^{27}Al-^{27}Al vector and the ^{27}Al EFG tensor to the crystal-fixed frame are both {0°, 0°, 0°}. Simulations were performed using SPINEVOLUTION software [43] for both an autocorrelation peak ($\Delta = 0$ kHz) and a cross peak ($\Delta = 2.5$ kHz), where Δ denotes the difference in isotropic chemical shifts of the two resonances.

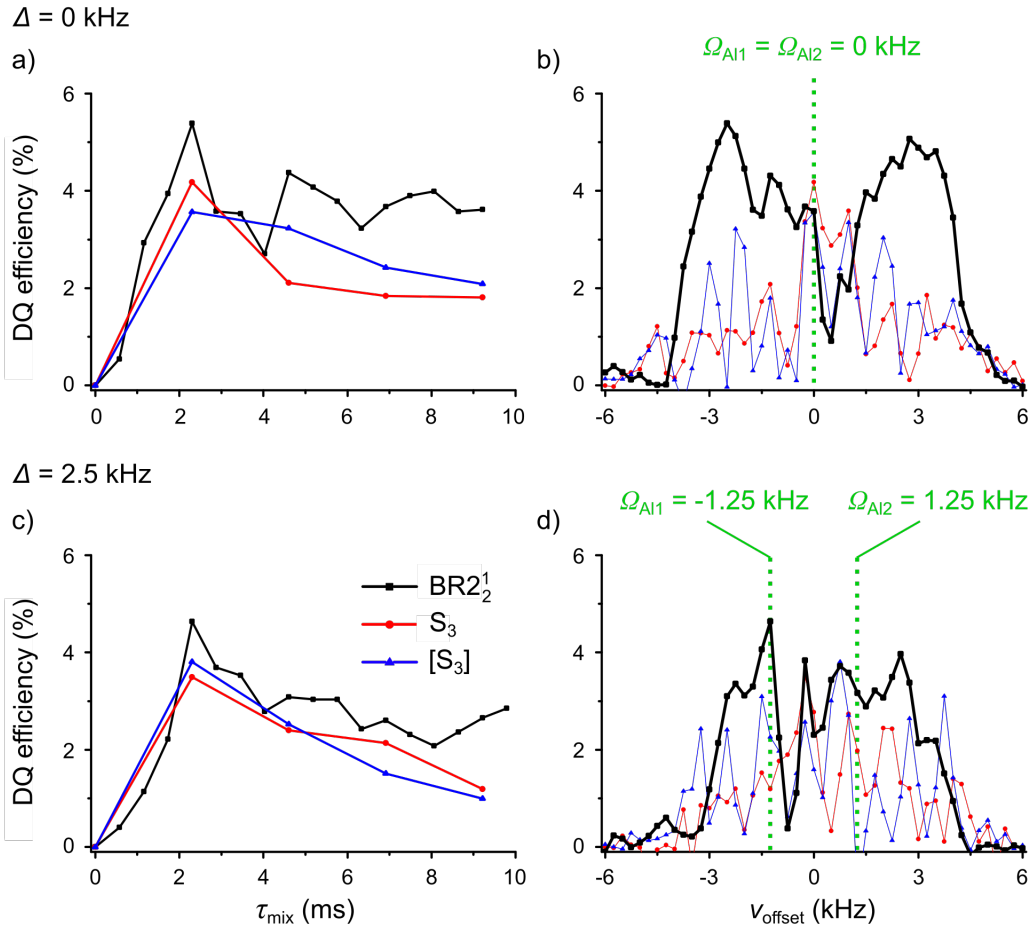

Figure 2. Plot of the simulated DQ efficiencies for $BR2_2^1$ (black squares), S_3 (red circles), and $[S_3]$ (blue triangles) recoupling as a function of (a, c) τ_{mix} and (b, d) ν_{offset} with τ_{mix} = 2.3 ms for a powder of ^{27}Al-^{27}Al pairs with (a, b) Δ = 0 (autocorrelation peak) and (c, d) Δ = 2.5 kHz (cross peak) at B_0 = 9.4 T with ν_R = 13.889 kHz and ν_{RF} = 2.32 kHz. In (a), ν_{offset} = 0 kHz for S_3 and $[S_3]$ and −2.5 kHz for $BR2_2^1$, whereas in (c) ν_{offset} = −1.25, −0.25 and 0.75 kHz for $BR2_2^1$, S_3 and $[S_3]$, respectively. Additional simulation parameters are given in section 6.2. The isotropic chemical shifts for Al_1 and Al_2 are both 0 kHz in (a,b) and −1.25 and 1.25 kHz, respectively in (c,d), as shown in (b, d). As both ^{27}Al nuclei are subject to C_Q of 3.0 MHz, the quadrupolar-induced shift (QIS) of each resonance is −0.53 kHz. The lines joining the points are used as a guide. In (b, d), the lines for $BR2_2^1$ are thicker for the sake of readability.

In Fig. 2a, the build-up of DQ coherence as a function of mixing time for an autocorrelation peak (Δ = 0 kHz) is shown. Although the optimal τ_{mix} is 2.3 ms for all recoupling sequences, the achieved DQ efficiencies are slightly different. For $BR2_2^1$, it is 5.5% (relative to a ^{27}Al signal acquired by a CT-selective π/2 pulse), while for S_3 and $[S_3]$, lower values of 4.0 and 3.5% are observed, respectively. However, such maximal DQ efficiency is still much lower than that for a pair of ^{13}C nuclei [40]. Because of this limited transfer efficiency, the acquisition of two-dimensional (2D) ^{27}Al-^{27}Al homonuclear dipolar correlation spectra often lacks sensitivity [39,44].

As shown in Fig. 2b, the optimal DQ efficiencies, for spin pairs with the same chemical shift (Δ = 0 kHz), are achieved for different ν_{offset} depending on the recoupling sequence. For both S_3 and $[S_3]$, we note the presence of strong oscillations at positive and negative ν_{offset} values, and that $\nu_{offset} \sim 0$ kHz yields the highest DQ efficiency. The situation is very different in the case of $BR2_2^1$ that displays a trough at ν_{offset} = 0.5 kHz, i.e. for on-resonance irradiation of the spin-pair (as the QIS is ~ −0.5 kHz). The DQ efficiency is larger when ν_{offset} deviates from 0 and optimum around ν_{offset} = −2.5 kHz and ν_{offset} = 3.5 kHz. The corresponding DQ bandwidth for $BR2_2^1$ spans about 9.0 kHz (from −4.0 to 5.0 kHz) with a trough at ν_{offset} = 0.5 kHz, whereas the RF-field amplitude is only equal to 2.3 kHz. Such bandwidth is considerably wider than those of both S_3 and $[S_3]$. In other words, $BR2_2^1$ is the most robust scheme to variations in isotropic chemical shift for autocorrelation peaks. The reasons for this notable robustness towards large offsets is clarified in sections 4.2 to 4.4.

Simulations for a cross peak with $\Delta \neq 0$ were also carried out. As the shift difference between a pair of tetra-coordinated Al and penta-coordinated Al (Al^{IV} and Al^{V}) or penta-coordinated Al and hexa-coordinated Al (Al^{V} and Al^{VI}) resonances is about 2.5 kHz at 9.4 T, the cross peak simulations were performed with Δ = 2.5 kHz. The DQ efficiency as a function of τ_{mix} for Δ = 2.5 kHz is presented in Fig. 2c, revealing an optimal τ_{mix} of 2.3 ms. The corresponding maximum DQ efficiency is 4.5% for $BR2_2^1$ and 3.5 and 3.8% for S_3 and $[S_3]$, respectively. Although these values are similar to the case Δ = 0 kHz (see Fig. 2a), the corresponding DQ bandwidth and offset profile are very different. Namely, the maximal efficiencies are achieved at ν_{offset} of −1.25, −0.25 and 0.75 kHz for $BR2_2^1$, S_3, and $[S_3]$ respectively. Hence, the observation of cross peaks ($\Delta \neq 0$) clearly requires a careful adjustment of ν_{offset}. We note that, unlike for Δ = 0 kHz (see Fig. 2a), the efficiency of $BR2_2^1$, S_3 and $[S_3]$ drops at longer mixing times. Hence, ^{27}Al 2D DQ-SQ homonuclear correlation spectra exhibit weak cross peaks between distant half-integer nuclei with distinct chemical shifts. Nevertheless, $BR2_2^1$ is much more robust with respect to offset variation and thus clearly outperforms S_3 and $[S_3]$, as shown in Fig. 2d. $BR2_2^1$ displays a bandwidth spanning ~ 7.5 kHz with two main troughs. The first one occurs for ν_{offset} around 0 to 0.5 kHz, and corresponds to an irradiation at the center of the two spin frequencies when accounting for quadrupolar induced shifts. In addition, in Fig. 2d, for which the starting operator is I_{1z}, the offset profile of $BR2_2^1$ shows a second notable minimum at ν_{offset} of ca. −0.75 kHz. This corresponds approximately to the on-resonance irradiation of the ^{27}Al nucleus with non-zero initial magnetization (i.e. $1I_{1z} + 0I_{2z}$) when accounting for the quadrupolar induced shift. Conversely, as seen in Fig. S1, when the other ^{27}Al nucleus has non-zero initial magnetization (i.e. $0I_{1z} + 1I_{2z}$), the notable minimum occurs at $\nu_{offset} \approx +1.75$ kHz, its resonance frequency. Further simulations (shown in Fig. S2) reveal that these two minima are observed when considering solely the first-order term of the quadrupolar interaction. The second-order term of the quadrupolar interaction only shifts the position of these minima by the QIS. As shown by numerical calculations of the density matrix in section 4.4, the presence of these troughs stems notably from the creation of unwanted SQ and triple-quantum (3Q) coherences of a single ^{27}Al

nucleus. In the case of S_3 and [S_3], it is worth noting that the DQ efficiency strongly oscillates as a function of ν_{offset}. Similar to the $BR2_2^1$ case, the minima correspond again to the creation of unwanted SQ and 3Q coherences of a single ^{27}Al spin. These oscillations have already been previously explained owing to interference between the first-order quadrupolar interaction and the RF pulses [41]. Simulations (reported in Fig. S3) clearly confirm this point but also prove that the dipolar interaction is involved. This is notably illustrated by comparing the oscillatory responses of S_3 and [S_3] when changing the relative orientation of the ^{27}Al EFG tensor to the crystal-fixed frame (see Figs. S3a and d) or the ^{27}Al-^{27}Al dipolar vector (see Figs. S3b and e) with respect to those in Figs. S3c and f, respectively. The positions of the minima are unchanged but their amplitudes can be strongly impacted by these tensor orientations (see Fig. S3).

In short, for both autocorrelation and cross peaks and at moderate ν_R (~ 14 kHz), $BR2_2^1$ is the most favorable choice since it provides the highest DQ efficiency and is the most robust to offset. Importantly, this remains valid for very fast MAS regimes (Fig. S4) and at higher magnetic fields (B_0 = 18.8 T, see Fig. S5). As the RF-field of $BR2_2^1$ is proportional to the MAS frequency, larger excitation bandwidth is observed at higher MAS frequencies. The maximal DQ efficiency for $BR2_2^1$ is only slightly reduced to 4.2% at a MAS frequency of 60 kHz compared to 5.0% at MAS frequency of 8 kHz, whereas those of S_3 and [S_3] decrease to 2.0 and 1.3%, respectively (see Fig. S4e).

3.2. Experimental results

To verify experimentally the superiority of $BR2_2^1$ for ^{27}Al homonuclear dipolar recoupling, we performed experiments on a mesoporous alumina (m-Al_2O_3) [39,45]. The 1D ^{27}Al NMR spectrum of m-Al_2O_3, acquired by a CT-selective $\pi/2$ pulse, is shown in Fig. 3a. It features three peaks, assigned to Al^{VI}, Al^{V}, and Al^{IV} sites, whose ^{27}Al shifts are at 7, 35, and 60 ppm, respectively. This is an interesting system for the examination of homonuclear dipolar recoupling sequences as it consists of three sites with substantial differences in quadrupolar interactions and shifts. Moreover, the shift difference between Al^{IV} and Al^{VI} sites is as large as 5 kHz at 9.4 T.

For our simulated ^{27}Al-^{27}Al system, the dipolar coupling constant of −0.3 kHz between two ^{27}Al nuclei is large enough for both S_3 and $[S_3]$ to reach optimal DQ efficiency after one sequence loop. However, for systems with longer distances between nuclei and/or with smaller gyromagnetic ratios, the dipolar coupling is accordingly smaller. Regarding this point, $[S_3]$ can be preferred to S_3 owing to the former's associated faster DQ build-up [40]. A faster build-up shortens the length of required recoupling periods and thus reduces the detrimental effects of DQ coherence dephasing during the excitation and reconversion blocks. Moreover, pure DQ recoupling can be preferred in multi-spin systems [29] and, as shown in simulations (Figs. 2b and 2d), $[S_3]$ has a similar offset profile to S_3. Therefore, we performed the experiments with $BR2_2^1$ and $[S_3]$ sequences.

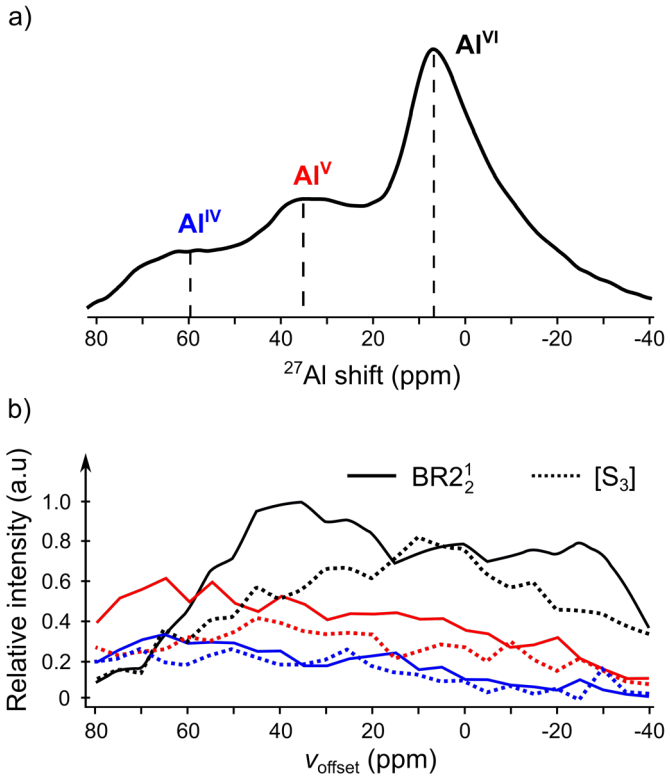

Figure 3. (a) 1D ^{27}Al direct excitation MAS NMR spectrum of m-Al_2O_3, featuring the three ^{27}Al sites, at B_0 = 9.4 T with ν_R = 13.889 kHz. The grey dashed lines indicate the centers of resonances associated to Al^{VI} (black), Al^{V} (red), and Al^{IV} (blue), sites resonating at 7, 35, and 60 ppm, respectively. (b) Plot of the experimental DQ efficiencies of the three ^{27}Al sites for $BR2_2^1$ (straight

lines) and [S_3] (dotted lines) recoupling using ν_{RF} = 2.3 kHz versus ν_{offset}. ν_{offset} is incremented from −40 to +80 ppm with a step of 5 ppm, to ensure coverage of the whole shift range of m-Al_2O_3. The experimental intensities are normalized to the maximum of the Al^{VI} site. The reader is referred to the web version for a color figure.

The experimental offset profiles of $BR2_2^1$ and [S_3] are presented in Fig. 3b. It is clearly confirmed that $BR2_2^1$ is more robust and efficient than [S_3]. The Al^{VI} site is taken as an example owing to its higher intensity (related to its greater presence in m-Al_2O_3) compared to the other two sites. While for $BR2_2^1$ the maximum DQ efficiency for Al^{VI} is achieved at ν_{offset} = 35 ppm (corresponding to an offset of −2.8 kHz), for [S_3] the optimal ν_{offset} is equal to 10 ppm, which corresponds closely to on-resonance irradiation for the Al^{VI} site. These results are in qualitative agreement with the simulations shown in Fig. 2b. Additionally, the maximum DQ efficiency of $BR2_2^1$ is 25% higher than that of [S_3], corresponding to a 56% reduction in required experimental time. The experimental gain in DQ efficiency for $BR2_2^1$ is comparable with the simulations reported in Fig. 2. The DQ efficiency of the Al^{VI} site shown in Fig. 3b includes the contribution of autocorrelation and cross peaks since the $^{27}Al^{VI}$ nuclei are coupled via dipolar interactions to other Al^{VI} sites (Δ = 0 kHz), Al^{V} sites (Δ = 2.8 kHz), and Al^{IV} sites (Δ = 5.5 kHz). It can be assumed from the numerical simulations (*vide supra*) that the experimental DQ efficiency for $BR2_2^1$ at ν_{offset} = 10 ppm mainly results from the excitation of ^{27}Al nuclei occupying Al^{V} and Al^{IV} sites, i.e. Al^{V}- Al^{VI} and Al^{IV}- Al^{VI} cross peaks resonating at the frequency of $^{27}Al^{VI}$ nuclei during the acquisition. The depth of the expected minima at ν_{offset} = 10 ppm is also decreased by the distributions of isotropic chemical shifts and quadrupolar parameters for the three ^{27}Al sites. This distribution of NMR parameters and the contribution of both autocorrelation and cross peaks to the experimental DQ-filtered signals reduce the oscillations of DQ efficiency as a function of offset for [S_3] with respect to the simulations shown in Fig. 2.

In summary, experiments at 9.4 T with ν_R ~ 14 kHz showed that for the studies of the spatial proximities between ^{27}Al nuclei with sizeable C_Q, $BR2_2^1$ is the most favorable choice of recoupling sequence. As an illustration, 2D homonuclear ^{27}Al through-space DQ-SQ correlation

NMR spectra of m-Al_2O_3 using $BR2_2^1$ recoupling at 9.4 T and 18.8 T are shown in Figs. S6a and b in the SI, respectively.

4. Theoretical descriptions

In contrast to ^{13}C-^{13}C systems [40], $BR2_2^1$ offers higher DQ efficiencies and better robustness to offset variations and chemical shift distributions than S_3 and $[S_3]$ for ^{27}Al-^{27}Al systems. Although numerical simulations match with experiments, the spin dynamics occurring under $BR2_2^1$ have not yet been fully understood, especially in that the homonuclear dipolar recoupling is seemingly facilitated by chemical shifts. Notably, the simulations presented in Fig. 2 have also shown the presence of troughs in the offset profiles corresponding to either irradiation in the middle of the two resonances, or irradiation on one (or two) of the two resonances. In this section, the influence of the offset on the DQ efficiency of the $BR2_2^1$ recoupling scheme is analyzed by deriving an effective Hamiltonian and by performing numerical simulations of spin dynamics. This section is organized as follows. Section 4.1 derives the average Hamiltonians of S_3, $[S_3]$, $R2_2^1$ and $R2_2^{-1}$ and explains why the average Hamiltonian theory (AHT) cannot be applied to describe the spin dynamics during the $BR2_2^1$ scheme. In section 4.2, we derive an effective Hamiltonian for the $BR2_2^1$ sequence in the offset-toggling frame. In section 4.3, we demonstrate that this effective dipolar coupling, with an amplitude modulated by the offsets of the coupled spins, can explain the trough in DQ efficiency profiles for both spin-1/2 and quadrupolar nuclei. More specifically, the dipolar scaling factor is reduced in the following cases: on-resonance irradiation of an autocorrelation peak or irradiation at the middle of the two resonances for a cross peak. However, it does not predict the trough in DQ efficiency for on-resonance irradiation of one of the two half-integer nuclei in the case of a cross peak (see Fig. 2d). Density matrix calculations shown in section 4.4 indicate that the trough in DQ efficiency when the $BR2_2^1$ scheme is applied on resonance stems from the creation of unwanted SQ and 3Q coherences. The lack of this trough for S_3 and $[S_3]$ is rationalized by comparing the excitation profiles of the $BR2_2^1$ and S_3 schemes in section 4.5.

4.1. Average Hamiltonian theory (AHT)

For the application of AHT [46], two conditions must be matched:

$$\begin{aligned} &\text{(i) Cyclicity:} && \mathrm{U_{RF}}(\tau_c) = \mathbf{1} \\ &\text{(ii) Periodicity:} && \mathrm{H_\lambda}(\tau_c + t) = \mathrm{H_\lambda}(t), \end{aligned} \tag{1}$$

where τ_c is the cycle time, which is rotor synchronized, and λ denotes either spin (chemical shift, dipolar or *J*-couplings) or RF interactions, H_λ and $\mathrm{U_{RF}}$ denotes the Hamiltonian of the interaction λ and the propagator of the RF interaction, respectively. As the two conditions mentioned above are met for the $\mathrm{R2}_2^1$ and $\mathrm{R2}_2^{-1}$ sequences, AHT can be used to calculate their effective Hamiltonians in the interaction frame of the RF-field. In this frame, the homonuclear dipolar coupling term in the first-order Hamiltonian is given by:

$$\bar{H}_{D,12}^{(1)} = b_{12} f_{12}(\beta_{PR}^{12}, \gamma_{PR}^{12})\{-4I_{1z}I_{2z} + (I_1^+ I_2^+ + I_1^- I_2^-) + (I_1^+ I_2^- + I_1^- I_2^+)\}, \tag{2}$$

where *D* denotes the dipolar coupling interaction, b_{12} is the dipolar coupling constant in rad.s^{-1}, and the scaling factor $f_{12}(\beta_{PR}^{12}, \gamma_{PR}^{12}) = \frac{3}{16\sqrt{2}} \sin(2\beta_{PR}^{12}) \cos(\gamma_{PR}^{12})$ in which β_{PR}^{12} and γ_{PR}^{12} are the Euler angles relating the $\mathbf{r}_{12}$ internuclear vector to the MAS rotor-fixed frame.

This Hamiltonian expression in Eq. 2 consists of a DQ term: $DQ_x = I_1^+ I_2^+ + I_1^- I_2^-$, a ZQ term: $ZQ_x = I_1^+ I_2^- + I_1^+ I_2^-$, and a longitudinal two-spin order term $2I_{1z}I_{2z}$. The term $f_{12}(\beta_{PR}^{12}, \gamma_{PR}^{12})$ represents a scaling factor. In the interaction frame of the RF-field, the isotropic shift terms in the first-order Hamiltonian are given by:

$\mathrm{R2}_2^1$

$$\bar{H}_{iso}^{(1)} = -\frac{2}{\pi}\left(\omega_{I_1} I_{1x} + \omega_{I_2} I_{2x}\right) = -4(\Omega_{I_1} I_{1x} + \Omega_{I_2} I_{2x}) \tag{3}$$

$\mathrm{R2}_2^{-1}$

$$\bar{H}_{iso}^{(1)} = \frac{2}{\pi}\left(\omega_{I_1} I_{1x} + \omega_{I_2} I_{2x}\right) = 4(\Omega_{I_1} I_{1x} + \Omega_{I_2} I_{2x}), \tag{4}$$

where ω_{I_i} and Ω_{I_i} with i = 1 or 2 denotes the isotropic chemical shift in rad.s^{-1} and Hz of I_i nucleus, respectively. The CSA terms in the first-order Hamiltonian of $R2_2^1$ and $R2_2^{-1}$ recoupling schemes are similar to Eqs. 3 and 4 but in the expression of these CSA terms, the recoupled CSA frequencies ω_{CSA,I_i} (or Ω_{CSA,I_i}) substitute ω_{I_i}(or Ω_{I_i}). The ω_{CSA,I_i} (or Ω_{CSA,I_i}) frequencies depend on the anisotropic chemical deshielding constants, σ_{aniso}^{i}, the asymmetry parameters of the CSA tensor, η_{CS}^{i} and the Euler angles describing the orientation of the principal axis-frame of the CSA tensor in the rotor-fixed frame.

As $BR2_2^1$ consists of n loops of $R2_2^1$ followed by n loops of $R2_2^{-1}$, a different number of n provides a different sequence [29,42]. Therefore, no basic periodic unit can be defined for $BR2_2^1$, implying that conventional AHT cannot be applied straightforwardly.

On the contrary, ($R2_8^1R2_8^{-1}$) is the basic periodic unit of both S_3 and [S_3]. $\bar{H}_{D,12}^{(1)}$ for S_3 is identical to that given in Eq. 2 while with the addition of two bracketing $\pi/2$ pulses, that of [S_3] is [40]:

$$\bar{H}_{D,12}^{(1)} = 2b_{12}f_{12}(\beta_{PR}^{12}, \gamma_{PR}^{12})DQ_x \quad (5)$$

Owing to the phase-inversion in the middle of the $R2_8^1R2_8^{-1}$ basic unit, the first-order chemical shift terms are suppressed. Regarding the first-order terms, it is worth mentioning that the only difference between $BR2_2^1$ and S_3 is the isotropic chemical shift terms. In the following section, the effect of these terms on the dipolar transfer process is investigated.

4.2. Analytical approximation in the offset-toggling frame

We first consider the case of ^{13}C nuclei with negligible CSA. As outlined above, the conventional AHT cannot be simply used in the case of $BR2_2^1$ owing to the lack of basic periodic unit. Nevertheless, one still can approximate its effective Hamiltonian using the first-order Hamiltonians of $R2_2^1$ and $R2_2^{-1}$derived in section 4.1 (Eqs. 2-4). To better understand the effect of first-order offset terms and their impact on the DQ efficiency, we transform $\bar{H}_{D,12}^{(1)}$ (Eq. 2) in the "toggling" frame defined by the first-order offset terms, using the following transformation:

$$U_{CS}\left(0,\underbrace{t}_{=2k\tau_R}\right)=e^{-i\bar{H}_{iso}^{(1)}t}$$
$$=\begin{cases} e^{\left(+i4\Delta t.\left(\frac{I_{1x}-I_{2x}}{2}\right)\right)}.e^{\left(+i4\Sigma t.\left(\frac{I_{1x}+I_{2x}}{2}\right)\right)} & 0<k\leq n \\ e^{\left(+i4\Delta(4n\tau_R-t).\left(\frac{I_{1x}-I_{2x}}{2}\right)\right)}.e^{\left(+i4\Sigma(4n\tau_R-t).\left(\frac{I_{1x}+I_{2x}}{2}\right)\right)} & n<k\leq 2n \end{cases} \quad (6)$$

where k is an integer, $\Delta = \Omega_{I_1} - \Omega_{I_2}$, and $\Sigma = \Omega_{I_1} + \Omega_{I_2}$. The dipolar coupling Hamiltonian of $BR2_2^1$ in the offset-toggling frame is:

$$\widetilde{H}_{D,BR2_2^1}^{\text{off-frame}}\left(\underbrace{t}_{=2k\tau_R}\right)=U_{CS}(0,t).\bar{H}_{D,12}^{(1)}.U_{CS}^{-1}(0,t) \quad \text{with} \quad 0<k\leq 2n \quad (7)$$

where "off-frame" denotes the offset-toggling frame. As $U_{CS}(0,4n\tau_R)=\mathbf{1}$, we are able to apply the Magnus expansion [47] to derive the analytical approximation of the dipolar interaction in this frame at the n^{th} point of $BR2_2^1$:

$$\bar{H}_{D,BR2_2^1}^{\text{off-frame}}(n)= A\begin{bmatrix} -\left(\mathrm{s}(4\Delta.2n\tau_R)+\mathrm{s}(4\Sigma.2n\tau_R)\right).2I_{1z}I_{2z} \\ +\left(1-\frac{1}{2}\left(\mathrm{s}(4\Delta.2n\tau_R)-\mathrm{s}(4\Sigma.2n\tau_R)\right)\right).ZQ_x \\ +\left(1+\frac{1}{2}\left(\mathrm{s}(4\Delta.2n\tau_R)-\mathrm{s}(4\Sigma.2n\tau_R)\right)\right).DQ_x \\ +\left(c(4\Sigma.2n\tau_R)+c(4\Delta.2n\tau_R)\right).2I_{1y}I_{2z} \\ +\left(c(4\Sigma.2n\tau_R)-c(4\Delta.2n\tau_R)\right).2I_{1z}I_{2y} \end{bmatrix} \quad (8)$$

where $A = b_{12}f_{12}(\beta_{PR}^{12},\gamma_{PR}^{12})$; $s(x)=\frac{\sin(x)}{x}$; and $c(x)=\frac{\cos(x)-1}{x}$. Note that the functions $\sin(x)/x$, and $(1-\cos(x))/x$, where x is a variable, are close to 0 when $x >> 1$, i.e. $n >> \nu_R/(8|\Delta|)$ or $\nu_R/(8|\Sigma|)$.

This calculation shows that during $BR2_2^1$, the effect of the offset terms can be seen as (i) generating additional single-quantum (SQ) terms: $2I_{1y}I_{2z}$ and $2I_{1z}I_{2y}$ and (ii) inducing a modulation of the scaling factors of each of the five terms present in Eq. 8. These scaling factors depend on the number of loops (n), the sum (Σ), and the difference (Δ) of chemical shifts of the two dipolar-coupled spins. It is important to note that the three former terms in Eq. 8 do not

commute with the SQ terms, and that they should thus be included in the DQ polarization transfer calculations.

Table 1. Amplitudes of the $BR2_2^1$ DQ and SQ terms present in Eq. 8 for the following three cases: irradiation in the middle of two distinct resonances ($\Delta \neq 0$, $\Sigma = 0$), off-resonance irradiation of an autocorrelation peak ($\Delta = 0$, $\Sigma \neq 0$), on-resonance irradiation for one of the two spins ($\Sigma = \pm\Delta$).

	DQ and SQ terms present in $\bar{H}_{D,BR2_2^1}^{off-frame}(n)$
$\Delta \neq 0$, $\Sigma = 0$	$A\left\{0.5[1 + \underbrace{s(4\Delta.2n\tau_R)}_{\sim 0 \text{ if } n \gg \nu_R/(8\lvert\Delta\rvert)}].DQ_x + \underbrace{c(4\Delta.2n\tau_R)}_{\sim 0 \text{ if } n \gg \nu_R/(8\lvert\Delta\rvert)}.(2I_{1y}I_{2z} - 2I_{1z}I_{2y})\right\}$
$\Delta = 0$, $\Sigma \neq 0$	$A\left\{1.5[1 - 1/3.\underbrace{s(4\Sigma.2n\tau_R)}_{\sim 0 \text{ if } n \gg \nu_R/(8\lvert\Sigma\rvert)}].DQ_x + \underbrace{c(4\Sigma.2n\tau_R)}_{\sim 0 \text{ if } n \gg \nu_R/(8\lvert\Sigma\rvert)}.(2I_{1y}I_{2z} + 2I_{1z}I_{2y})\right\}$
$\Sigma = \pm\Delta$	$A\left\{1.0DQ_x + \underbrace{c(4\Sigma.2n\tau_R)}_{\sim 0 \text{ if } n \gg \nu_R/(8\lvert\Sigma\rvert)}.[(2I_{1y}I_{2z} + 2I_{1z}I_{2y}) \pm (2I_{1y}I_{2z} - 2I_{1z}I_{2y})]\right\}$

The first case ($\Delta \neq 0$ kHz, $\Sigma = 0$ kHz) corresponds to a cross peak, for which the RF irradiation is applied at the center of the two resonances. As $\Sigma = 0$, $s(4\Sigma.2n\tau_R)$ is 1. Furthermore for $n \gg \nu_R/(8|\Delta|)$, both $s(4\Delta.2n\tau_R)$ and $c(4\Delta.2n\tau_R)$ are close to 0, which results in a scaling factor of about $0.5f_{12}(\beta_{PR}^{12}, \gamma_{PR}^{12})$. The second case ($\Sigma \neq 0$ kHz, $\Delta = 0$ kHz) corresponds to the off-resonance irradiation of an autocorrelation peak. In that case, the scaling factor, provided that $n \gg \nu_R/(8|\Sigma|)$, is about 3-fold larger than in the first case. For the third case, Δ and Σ can be arbitrarily chosen as long as they are identical in absolute value. This case corresponds to the on-resonance irradiation of (at least) one of the two resonances. In that case, the scaling factor is about 2-fold larger than in the first case, and about a factor of 2/3 lower than in the second case.

Based on this crude analysis, we expect the first case to build-up slowly and the second case to build-up rapidly.

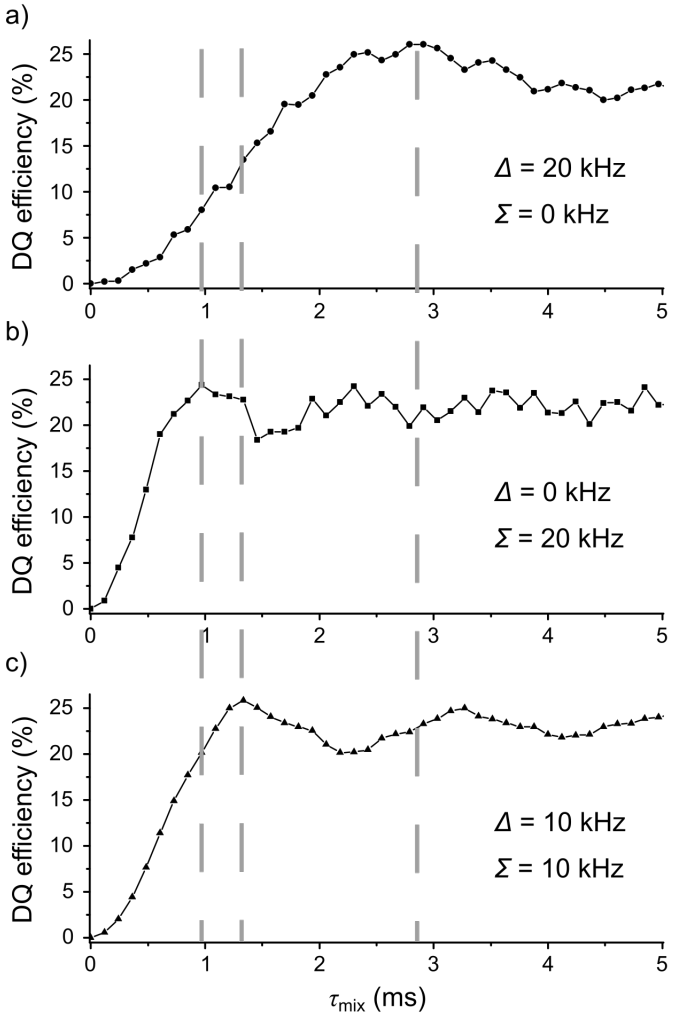

Figure 4. Numerical simulations of DQ efficiencies are plotted versus τ_{mix}, obtained with $BR2_2^1$ with ν_{RF} = 33 kHz on a powder of ^{13}C-^{13}C pairs. The spin system consists of two ^{13}C nuclei at B_0 = 9.4 T with ν_R = 66 kHz. The $b_{12}/(2\pi)$ constant between the two ^{13}C nuclei is −2.0 kHz. No ^{13}C CSA was included. The simulated DQ build-up curves were performed at the different conditions listed in Table 1: (a) Δ = 20 kHz, Σ = 0 kHz; (b) Δ = 0 kHz, Σ = 20 kHz; and (c) $\Delta = \Sigma$ = 10 kHz. The dashed lines indicate the optimal τ_{mix} of each case. The lines joining the points are used as a guide.

This is further illustrated in Fig. 4, which shows numerical simulations corresponding to the three cases presented in Table 1. The optimal τ_{mix} for the three simulated cases, as indicated by the dashed lines in Fig. 4, are 2.9, 1.0, and 1.3 ms for Δ = 20 kHz and Σ = 0 kHz; Δ = 0 kHz and Σ = 20 kHz; and $\Delta = \Sigma$ = 10 kHz, respectively. This is in good agreement with the analytical results presented in Table 1. A smaller scaling factor leads to a slower build-up of the DQ coherence, and hence a reduced DQ efficiency at short mixing times.

A similar analysis can be carried out for a pair of ^{13}C nuclei subject to CSA as well as the dipolar interaction. $\bar{H}_{D,12}^{(1)}$ can be expressed in a chemical shift-fixed frame, in which the ^{13}C coherences do not evolve under offset and CSA as $U_{CS}(0, 4n\tau_R) = U_{CSA}(0, 4n\tau_R) = \mathbf{1}$, by applying the transformation of Eqs. 6 and 7 with $\Delta = \Omega_{I_1} + \Omega_{\mathrm{CSA,I_1}} - \Omega_{I_2} - \Omega_{\mathrm{CSA,I_2}}$, and $\Sigma = \Omega_{I_1} + \Omega_{\mathrm{CSA,I_1}} + \Omega_{I_2} + \Omega_{\mathrm{CSA,I_2}}$. In that case, Δ and Σ frequencies depend on the crystallite orientations in the rotor. Eq. 8 and Table 1 remain valid in the presence of CSA but the position and intensity of the trough will depend on the crystallite. Hence, the powder average decreases the depth of the trough for Σ = 0. In order to verify this, we performed simulations on an isolated ^{13}C-^{13}C system with Δ = 2.5 kHz and with different CSA values. The simulated offset profiles (given in Fig. S7) indeed do not show the trough in DQ efficiency at the center of two ^{13}C resonances, except for a CSA of 0 kHz (see Fig. S7a). These simulations confirm the elimination of the trough at Σ = 0 in the presence of CSA.

4.3.The sufficiency of the analytical approximation

This section investigates the limits of the analytical approximation derived in the previous section to describe the spin dynamics during $\mathrm{BR2}_2^1$ recoupling, firstly for spin-1/2 nuclei and then for half-integer quadrupolar nuclei.

4.3.1. Spin-1/2 nuclei

We compared the offset profiles computed using analytical expressions of the $\mathrm{BR2}_2^1$ effective Hamiltonians (MATLAB v7.8 [48]) to that simulated using spin dynamics numerical software

(SPINEVOLUTION). For the former approach, the initial operator I_{1z} is subjected to a unitary propagator, calculated from (i) the first-order AHT terms of $R2_2^1$ and $R2_2^{-1}$ (Eqs. 2, 3, and 4) and (ii) the analytical approximation of $BR2_2^1$ (Eq. 8); then the expectation value of the I_{2z} operator is subsequently calculated. The offset profiles were obtained by performing the aforementioned procedure at different offset values. Following the previous section, three cases (with $\Sigma = 0$ kHz, $\Delta = 0$ kHz, and $\Sigma = \Delta$) were considered. In all cases, the offset profiles were simulated at τ_{mix} = 0.97 ms (or $n = 8$).

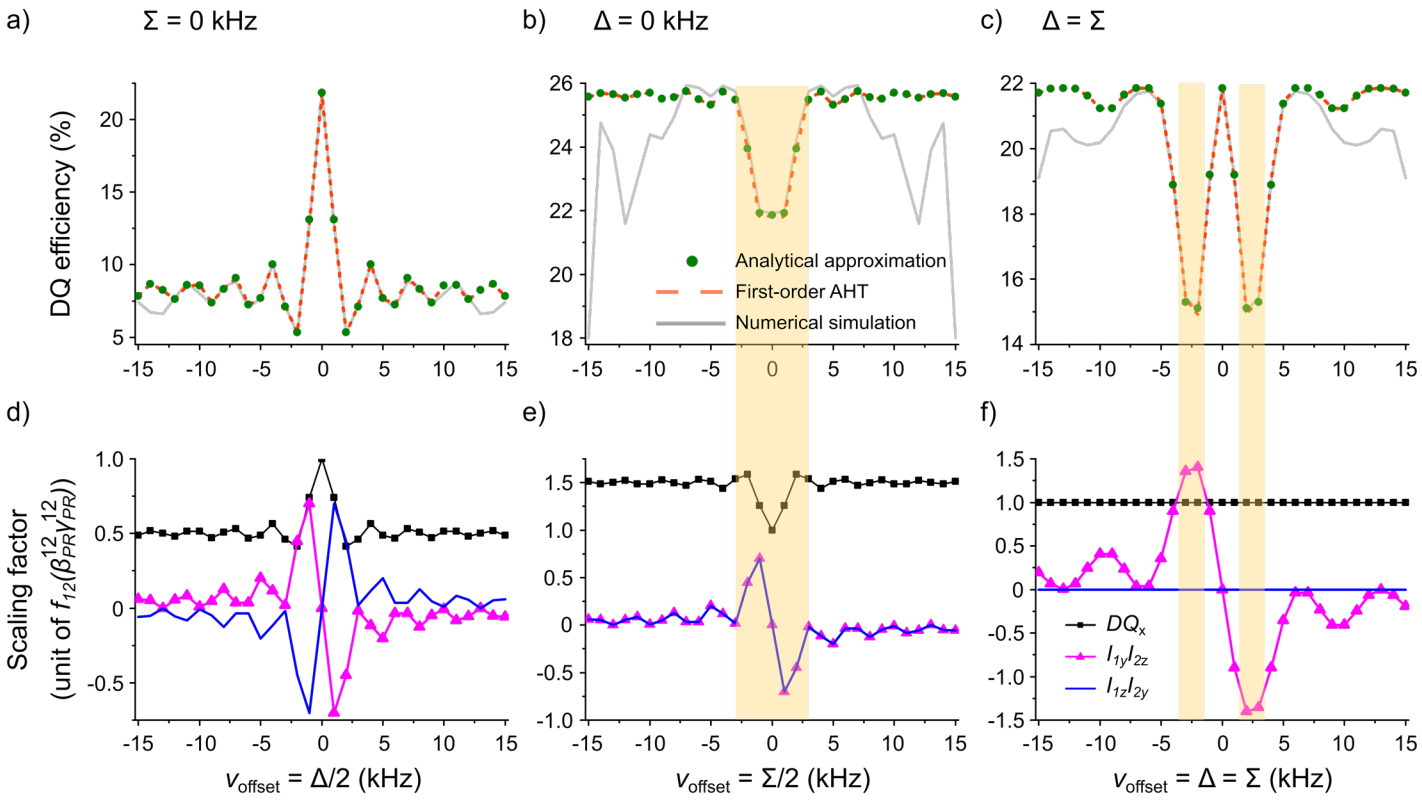

Figure 5. (a-c) Plot of the DQ efficiencies of $BR2_2^1$ recoupling with ν_{RF} = 33 kHz as a function of ν_{offset} for a powder of ^{13}C-^{13}C pairs at B_0 = 9.4 T with ν_R = 66 kHz, calculated by three different methods: the analytical approximation of $BR2_2^1$ in the offset-toggling frame (Eq.8) (green circles), the first-order AHT terms of $R2_2^1$ and $R2_2^{-1}$ (Eqs. 2, 3, and 4) (orange dashed line), and numerical simulations (grey straight line). (d-f) Plot of the scaling factors of DQ and SQ terms as a function

of ν_{offset} corresponding to the three cases in (a-c). The color strips in (b-c, e-f) simultaneously highlight the troughs in DQ efficiency and the maxima of SQ terms in absolute value. These offset and scaling factor profiles were calculated and simulated for (a,d) $\Sigma = 0$ kHz, (b,e) $\Delta = 0$ kHz, and (c,f) $\Delta = \Sigma$; all at $\tau_{mix} = 0.97$ ms ($n = 8$). The isotropic chemical shifts for $^{13}C_1$ and $^{13}C_2$ nuclei are (a,d) $\pm \nu_{offset}$, (b,e) $-\nu_{offset}$, and (c,f) 0 and ν_{offset}, respectively or vice versa. The spin system and simulation parameters are identical to those of the simulations shown in Fig. 4.

Figs. 5a-c compares the offset profiles calculated from the first-order AHT terms of $R2_2^1$ and $R2_2^{-1}$, the analytical approximation, and numerical simulations. The first thing to note is that the two former approaches are in perfect agreement, which validates the use of Eq. 8. Moreover, these analytical approaches provide very similar offset profiles to numerical simulations, particularly for moderate offsets, validating the use of these analytical approximations. The main features can be well reproduced, notably the trough in DQ efficiency for on-resonance irradiation of an autocorrelation peak ($\Delta = 0$, see Fig. 5b). This trough indicates that offset promotes homonuclear dipolar recoupling in the case of the $BR2_2^1$ sequence, contrary to common recoupling techniques, for which offsets reduce the recoupling efficiency. Furthermore, there is also a good agreement between offset profiles calculated using analytical approximations and numerical simulations when $\Sigma = 0$ and $\Sigma = \Delta$ (Figs. 5a and c, respectively) as well as for other cases (shown in Fig. S8). In particular, Figs. S8c and d show a decreased DQ efficiency for a cross peak, when the irradiation is applied near the middle of the two resonances. This trough demonstrates again that the offset promotes the homonuclear dipolar recoupling in the case of the $BR2_2^1$ scheme. The deviations that do occur between the analytical approximations and the numerical simulations at large ν_{offset} ($|\nu_{offset}| \geq 7.0$ kHz in Figs. 5b-c) are attributed to higher-order terms, illustrating the limits of the analytical approximation conducted here since only first-order terms are retained. Nevertheless, it is sufficient to explain the main features of the spin dynamics of $BR2_2^1$.

Since SQ and DQ terms do not commute with each other, it is interesting to know how the SQ terms affect the DQ efficiency. Such understanding can provide a qualitative explanation for the patterns of the offset profiles. For that purpose, we plot the scaling factor of both the DQ and SQ terms as a function of ν_{offset}, as shown in Fig. 5d-f. It is revealed that whenever the SQ terms

reach a maximum in absolute value, the DQ efficiency is reduced (highlighted region). This is particularly evident for $\Delta = \Sigma$ (see Figs. 5c and f) where the presence of the two troughs at $|\nu_{offset}|$ = 2.0-3.0 kHz (Fig. 5c) exactly correspond with the maxima of SQ terms (Fig. 5f). This illustrates the detrimental effect of the SQ terms on the DQ polarization transfer.

As mentioned above, the derived analytical approximations only contain first-order terms and are not sufficient to estimate the DQ excitation bandwidth for $BR2_2^1$. Nevertheless, this can be done using SPINEVOLUTION by plotting 2D maps, as shown in Fig. 6. The maps confirms the presence of a trough at $\Sigma = 0$, i.e. for the on-resonance irradiation of an autocorrelation peak or an irradiation centred between the two resonances for a cross peak. When $\Sigma \neq 0$, the DQ efficiency is higher for an autocorrelation peak than a cross peak, in agreement with Figs. 4 and 5 and the scaling factor reported in Table 1. The derived analytical approximation can describe the spin dynamics of the $BR2_2^1$ sequence (at moderate ν_{offset}) for spin-1/2 nuclei. This is also valid for half-integer quadrupolar nuclei with very small C_Q, for which the RF-field magnitude is much larger than the quadrupolar frequency in the principal axis system of the EFG tensor, $\nu_Q = 3C_Q/(4I(2I-1))$: $\nu_{RF} \gg \nu_Q$ (see section S2.2 in the SI and Figs. S9-10).

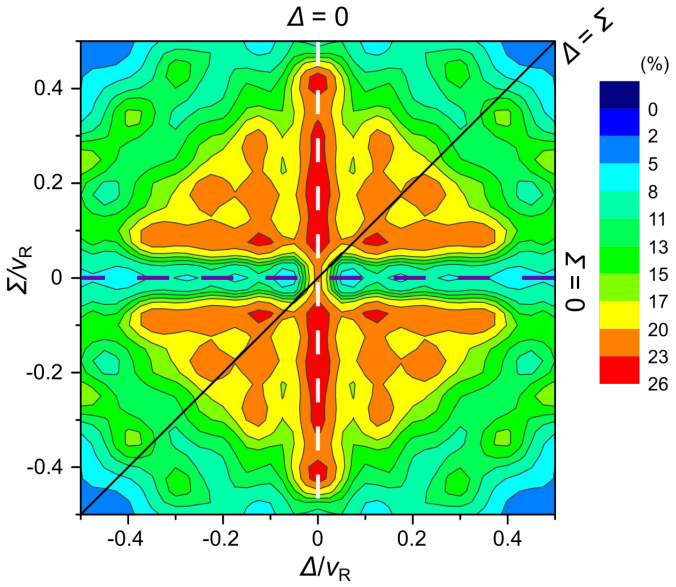

Figure 6. Simulated DQ efficiency for $BR2_2^1$ as a function of the sum (Σ) and difference (Δ) of two ^{13}C chemical shifts of a powdered ^{13}C-^{13}C spin-pair system. The $b_{12}/(2\pi)$ constant between the two ^{13}C nuclei is −2.0 kHz. The simulation was carried out at B_0 = 9.4 T with ν_R = 66 kHz and ν_{RF} = 33 kHz and τ_{mix} = 0.97 ms (n = 8). The three cases in Figs. 4 and 5 are highlighted, $\Sigma = 0$ (horizontal violet dashed line), $\Delta = 0$ (vertical white dashed line), and $\Delta = \Sigma$ (diagonal black straight line).

4.3.2. Half-integer quadrupolar nuclei

The analytical approximation approach can be extended to the half-integer quadrupolar nuclei case because under large quadrupolar interaction compared to the RF-field (i.e. $\nu_{RF} \ll \nu_Q$), one often assumes that the spin dynamics can be described in the CT subspace [16,18]. A mathematical treatment similar to the one reported in section 4.2 can be conducted and the analytical approximation of $BR2_2^1$ for a dipolar-coupled half-integer quadrupolar spin pair with spin number I is reported in Eq. S5 in the SI. The important modification, compared to the spin-1/2 case in Eq. 8, is that the effective dipolar coupling in the CT subspace is scaled by the factor $\left(\frac{2}{3}+\frac{1}{3}\left(I+\frac{1}{2}\right)^2\right)$. This scaling factor is numerically verified by simulations, as shown in Fig. S12. As explained above, this calculation clarifies the involvement of the offset terms in DQ magnetization transfer during the $BR2_2^1$ spin dynamics, thus explaining the broad offset profile of $BR2_2^1$ as compared to S_3 and $[S_3]$.

Nevertheless the $BR2_2^1$ spin dynamics, detailed in section 4.3 and/or Eq. S5, cannot *fully* explain the intense trough observed in Figures 2d, S1, and S2 ($\Delta \neq 0$ kHz) for on-resonance irradiation of the spin bearing the initial magnetization. This feature, which is not observed for spin-1/2 nuclei, cannot be explained by tracking the $BR2_2^1$ spin dynamics in the CT subspace and is investigated below using numerical simulations.

4.4. Leakage from the CT subspace and DQ_{CT} efficiency loss

The origin of these troughs can be investigated by calculating the density matrices for a powder of a single ^{27}Al nucleus under the application of the first $BR2_2^1$ recoupling block ("DQ exc") at different ν_{offset}. The results are shown in Fig. 7, together with similar simulations

performed on the S_3 and $[S_3]$ recoupling sequences. To simplify the analysis, the quadrupolar interaction is only considered up to the first-order. Fig. 7 shows the plot of the norm of coherences, the I_z magnetization and population differences between energy levels m_I and $-m_I$ as a function of ν_{offset}. The coherences can be classified as (i) SQ (between energy levels m_I and m_I+1 with m_I of −5/2 and 3/2 for the second ST (SQ_{ST2}), −3/2 and 1/2 for the first ST (SQ_{ST1}), and −1/2 for the CT (SQ_{CT})), (ii) DQ (between energy levels m_I and m_I+2 with m_I of −5/2, −3/2, −1/2, and 1/2) involving the satellite transitions (DQ_{STs}), (iii) 3Q (between m_I and m_I+3 with m_I of −5/2, −3/2, and −1/2), (iv) quadruple-quantum (4Q) (between m_I and m_I+4 with m_I of −5/2 and −3/2), and (v) quintuple-quantum (5Q) (between energy levels $m_I = -5/2$ and $m_I = +5/2$).

At an on-resonance condition (ν_{offset} = 0 kHz), $BR2_2^1$ creates 3Q coherences. For ν_{offset} = ±0.25 kHz, SQ_{CT} coherences are also produced. The creation of these unwanted coherences is associated to a decrease of the longitudinal magnetization (see Figs. 7a and d), which results in a reduction of the DQ_{CT} efficiency for the on-resonance irradiation of an excited (dipolar coupled) nucleus. This effect explains the trough in DQ_{CT} efficiency for a cross peak when the offset is on-resonance with one (or both) of the two half-integer-spin quadrupolar nuclei (Figs. 2b, 2d, S1, and S2). Furthermore, it also further reduces the DQ_{CT} efficiency for on-resonance irradiation of an autocorrelation peak for half-integer quadrupolar nuclei. As the STs are broad, they are not efficiently excited by the $BR2_2^1$ scheme and the norm of the related SQ coherences are low. For $|\nu_{offset}| \geq 3$ kHz, the effective RF-field during the CT-selective π pulses of the $BR2_2^1$ scheme deviates from the y-axis, leading to an incomplete inversion of the CT magnetization. Consequently, SQ_{CT} coherences are created, which further reduces the longitudinal magnetization, and thus the DQ_{CT} efficiency of $BR2_2^1$ recoupling.

For comparison, similar simulations were carried out for small C_Q values (see Fig. S13). In this case, the application of the $BR2_2^1$ scheme on-resonance does not produce the unwanted SQ_{CT} and 3Q coherences, explaining the absence of the trough in DQ efficiency for on-resonance irradiation of the excited nucleus (see Figs. S9c and d and S10). Furthermore, as the width of the STs is comparable to the excitation bandwidth of the pulses, SQ coherences of the two STs are

excited besides that of the CT, in contrast with the case of large C_Q values (compare Figs. 7a and S13).

For the S_3 and [S_3] sequences, the amount of 3Q coherences created with on-resonance irradiation is much smaller than for $BR2_2^1$ and the longitudinal magnetization is accordingly preserved (see Figs. 7b and c, respectively). Therefore, they do not exhibit a trough at the on-resonance frequency of the excited nucleus. However, both S_3 and [S_3] schemes create a substantial amount of 3Q and SQ_{CT} coherences for $|\nu_{offset}| \geq 1$ kHz. The creation of these unwanted terms goes with a decrease of the longitudinal magnetization and hence, of the DQ_{CT} efficiency. In particular, the local minima of the longitudinal magnetization at $\nu_{offset} = \pm 1$ and ± 2.5 kHz for S_3 recoupling explains its troughs in DQ efficiency seen in Fig. 2b (taking into account the QIS due to the second-order quadrupolar interaction, which is not considered in Fig. 7).

Fig. 7 clearly shows that for large C_Q values, the $BR2_2^1$ scheme is more efficient than S_3 and [S_3] for the creation of 3Q coherences at $\nu_{offset} = 0$ kHz, which contributes to the difference in DQ efficiency for the on-resonance irradiation of the excited (dipolar coupled) nucleus. It must be noted that for all recoupling sequences, the created 3Q coherences almost exclusively correspond to those between energy levels $m_I = -3/2$ and $m_I = +3/2$ (simulations not shown), i.e. between the two ST_1. Therefore, the creation of these 3Q coherences when the $BR2_2^1$ sequence is applied on-resonance is associated with the decrease of the population differences between energy levels +3/2 and −3/2 as well as +1/2 and −1/2, owing to the irradiation of the ST_1 (see Fig. 7d). This process is analogous to the creation of DQ coherences for a spin-1 nucleus, such as ^{14}N, by applying the $R2_2^1$ scheme on-resonance (see the section S2.4 of the SI) [49].

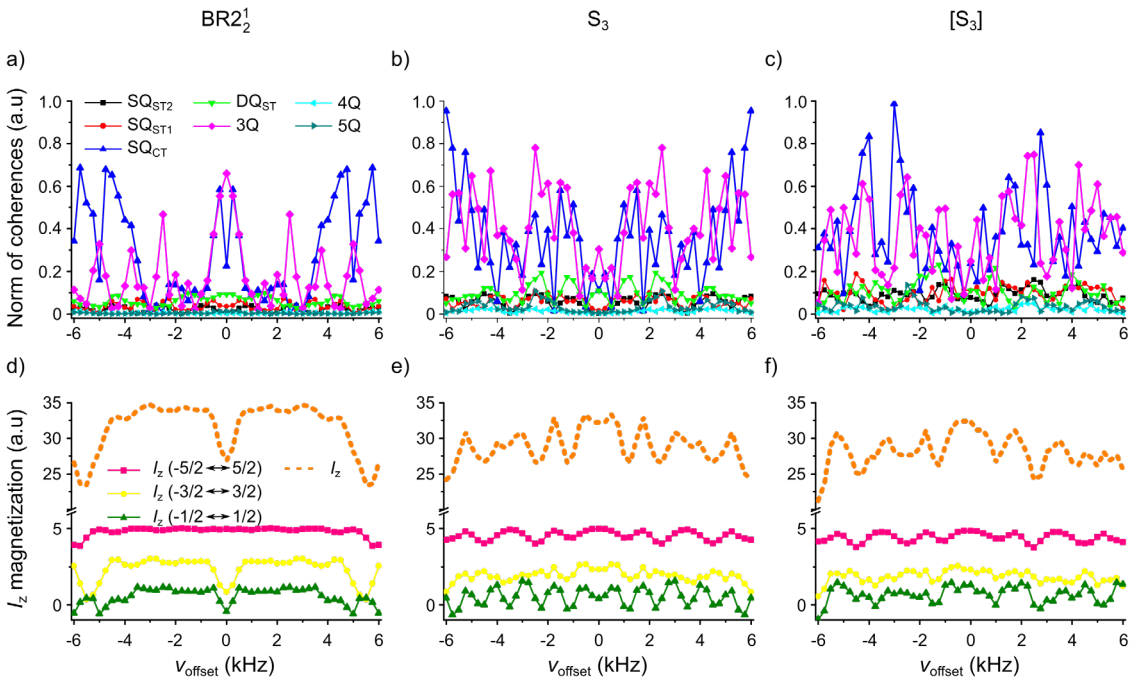

Figure 7. Calculated norm of coherences (a-c) and I_z magnetization (d-f) as a function of ν_{offset} for a powder of an isolated ^{27}Al nucleus after a BR2$_2^1$ (a,d), S$_3$ (b,d), or [S$_3$] (c,f) recoupling of τ_{exc} = 1.15 ms. For (a-c), the coherences are: SQ$_{ST2}$ (black squares), SQ$_{ST1}$ (red circles), SQ$_{CT}$ (blue triangles up), DQ$_{STs}$ (green triangles down), 3Q (magenta diamonds), 4Q (cyan triangles left), and 5Q (dark cyan triangles right). For (d-f), the I_z magnetization (dashed orange line), as well as the population differences between the energy levels m_I and $-m_I$ with m_I = 1/2 (dark green triangles), 3/2 (yellow circles) and 5/2 (e-f) are presented. Calculations were performed at B_0 = 9.4 T with ν_R = 13.889 kHz and ν_{RF} = 2.32 kHz. The ^{27}Al isotropic chemical shift and C_Q are 0 kHz and 3.0 MHz, respectively. The lines joining the points are used as a guide.

4.5. Excitation profiles of recoupling sequences

In order to investigate further the excitation of the STs by BR2$_2^1$ and S$_3$ recoupling, we analyzed the excitation profile of these schemes by calculating the Fourier Transform (FT) of the RF-field $\nu_{RF}(t)$ in the rotating frame (see Fig. 8). The R2$_2^1$ scheme can be described as the sum of two trains of π pulses with opposite phases and shifted in time by τ_R, i.e. two interleaved DANTE trains [49,50]. Hence, the FT of each DANTE train with a period $2\tau_R$ is a train of RF spikelets

separated by $\nu_R/2$. Whereas the spikelets of the first DANTE train are all in phase, those of the second DANTE train alternate because of the time shift by τ_R. As the two DANTE trains have opposite phases, the centerband and all even sidebands vanish. Solely the odd sidebands separated by ν_R remain. In the case of the $BR2_2^1$ scheme, the phase shift by 180° at the midpoint of the sequence produces an additional modulation at $2/(\tau_{mix}) \approx 1.74$ kHz for $\tau_{mix} = 1.15$ ms (see Fig. 8a). Furthermore, as the RF-field $\nu_{RF}(t)$ is an even function for $BR2_2^1$, its FT is an even real function. The calculated excitation profile of $BR2_2^1$ indicates that this scheme excites STs in a symmetric manner when it is applied on-resonance. It has been shown that a symmetric irradiation of the STs in the manner of fast amplitude modulated (FAM) pulses can efficiently convert the longitudinal magnetization of a single quadrupolar nucleus with $I \geq 3/2$ into 3Q coherences [51]. In fact, the $R2_2^1$ scheme is a particular case of the FAM-II pulse [52].

The excitation profile of the S_3 scheme is shown in Fig. 8b. Since $\nu_{RF}(t)$ is a real function, which is neither odd nor even, its FT is the sum of an even real function and an odd pure imaginary function, which both exhibit modulations at $2\nu_R = 27.8$ kHz and $\nu_R/8 \approx 1.7$ kHz associated to the lengths of the $\pi/2$ pulses and $R2_8^1$ scheme, $\tau_R/2$ and $8\tau_R$, respectively. The largest RF spikelets at $\pm 3\nu_R/16$ and $\pm 5\nu_R/16$ are imaginary and those at positive and negative frequencies are antiphase. Hence, when applied on-resonance, the S_3 scheme mainly achieves an antisymmetric irradiation of the STs, which does not create 3Q coherences. Therefore, the S_3 and $[S_3]$ schemes are less efficient than the $BR2_2^1$ scheme to create 3Q coherence with on-resonance irradiation. Furthermore, when a RF spikelet of S_3 irradiates the CT, SQ_{CT} are excited. This phenomenon explains the maxima in SQ_{CT} for $\nu_{offset} = \pm\nu_R/16 = \pm 0.9$ kHz and $\pm 3\nu_R/16 = \pm 2.5$ kHz in Fig. 7b and the oscillation of the population difference between energy levels 1/2 and −1/2 as function of offset in Fig. 7e.

Furthermore, in order to investigate the influence of MAS frequency on the spin dynamics during the $BR2_2^1$, S_3 and $[S_3]$ schemes, we also simulated the norm of the coherences, the longitudinal magnetization and population differences between energy levels m_I and $-m_I$ for a powder of a single ^{27}Al nuclear environment as a function of ν_{offset} at $\nu_R = 60$ kHz (see Fig. S14).

In order to interpret these simulations, we also calculated the excitation profile of these recoupling schemes at this MAS frequency (see Fig. S15). These results discussed in subsection S2.5 of the Supporting Information explain why higher MAS frequencies decrease the DQ efficiency of the S_3 and $[S_3]$ sequences but barely affect that of $BR2_2^1$ recoupling.

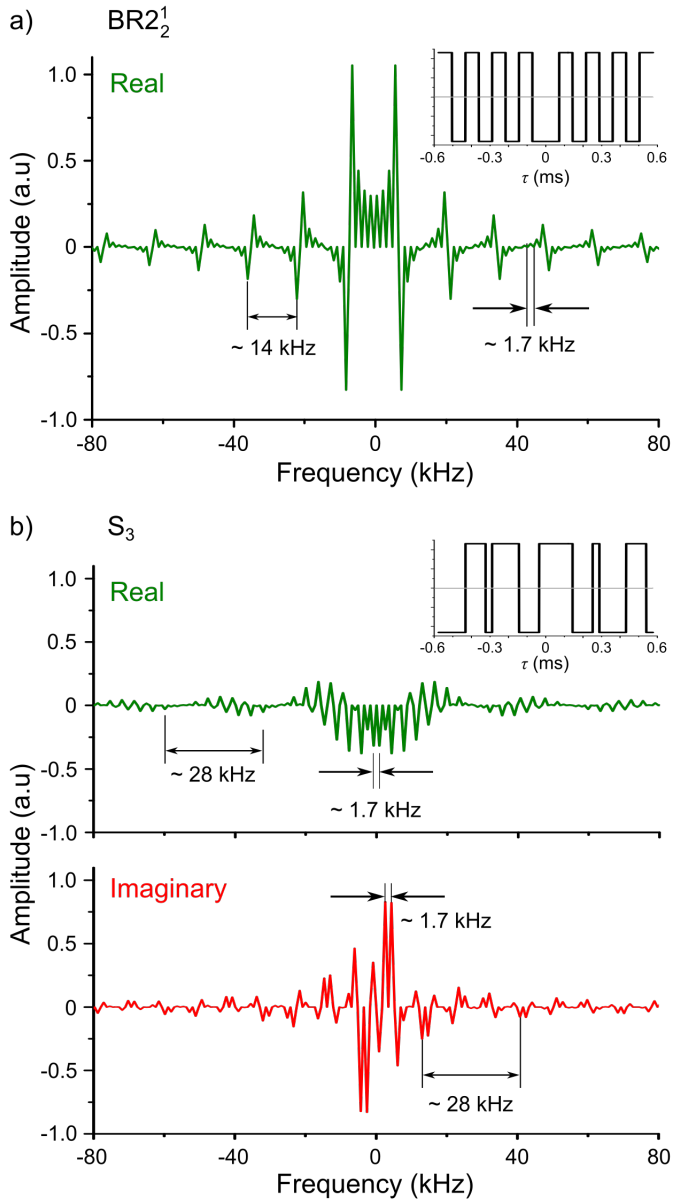

Figure 8. Excitation profile of the (a) $BR2_2^1$ and (b) S_3 sequences with a length of 1.15 ms at ν_R = 13.889 kHz. The $\nu_{RF}(t)$ functions for $BR2_2^1$ and S_3 are shown in the insets of (a) and (b), respectively. The time t = 0 was chosen as the middle of (a) $BR2_2^1$ and (b) S_3 schemes. The imaginary part of the $BR2_2^1$ excitation profile is not displayed since it is null.

5. Conclusion

We have numerically compared three similar yet different homonuclear dipolar recoupling sequences: $BR2_2^1$, S_3, and $[S_3]$. Their efficiencies for exciting DQ coherences between the CTs of two dipolar-coupled ^{27}Al nuclei under MAS were evaluated. The numerical results were supported by experiments performed on m-Al_2O_3 and it was shown that, compared to S_3 and $[S_3]$, $BR2_2^1$ is a favorable choice owing to its higher achieved DQ efficiency and robustness to offset variations and isotropic shift distributions. The better performance of this sequence originates from the involvement of chemical shifts in facilitating the magnetization transfer. For a better understanding of this particular magnetization transfer mechanism, theoretical treatments were employed. Under a hard-pulse regime (relatively small quadrupolar interaction), a similar pattern of offset effects for a ^{27}Al-^{27}Al pair under $BR2_2^1$ is also observed for spin-1/2 systems. An AHT approach cannot straightforwardly be applied to $BR2_2^1$ owing to the absence of a basic periodic unit, thus we rewrote the dipolar coupling Hamiltonian in an offset-toggling interaction frame where an analytical approximation can be derived. This expression, whose viability was verified by numerical simulations at specific conditions (small isotropic chemical shifts and without CSA terms), not only explains the trough in DQ efficiency at the center of two resonances, but also clarifies the relationship between offset and DQ efficiency for a pair of spin-1/2 nuclei. It shows that for maximum DQ transfer efficiency, ν_{offset} should be set away from the center of the two isotropic shift resonances. The applicability of the analytical approximation can also be extended to half-integer-spin quadrupolar nuclei in the CT subspace. However, it fails to explain the trough in DQ efficiency at on-resonance irradiation of an excited quadrupolar nucleus when subjected to a relatively large quadrupolar interaction. In this case, density matrix calculations were used to explain this phenomenon, which is notably due to the creation of 3Q coherences by $BR2_2^1$ for on-resonance irradiation of a single ^{27}Al nucleus. Such a feature is not observed for S_3 and $[S_3]$ recoupling. We have shown that $BR2_2^1$ efficiently excites the 3Q coherences because it irradiates the STs in a symmetric manner, unlike S_3. These unwanted terms interfere destructively with the

build-up of the desired DQ_{CT} term between two coupled half-integer-spin quadrupolar nuclei. The excitation profile of $BR2_2^1$ also explains why its DQ efficiency does not depend heavily on the MAS frequency, unlike S_3. Owing to the efficient suppression of the offset terms up to third-order, the supercycled S_3 and $[S_3]$ schemes can work well within a given ν_{offset} range for spin-1/2 nuclei. Unfortunately, this feature is not valid for quadrupolar nuclei with large quadrupolar interactions since at off-resonance conditions, these recoupling schemes generate a substantial amount of unwanted terms (see Figs. 7b-c), leading to inefficient DQ transfer. For the $BR2_2^1$ sequence, on the other hand, the offset is still retained in the first-order approximation and is involved in the DQ polarization transfer, with off-resonance irradiation generating a lower amount of unwanted coherences (see Fig. 7a), enhancing the overall DQ transfer efficiency and robustness. These findings can potentially lead to novel strategies in designing pulse sequences where usually-unwanted terms should be preserved for superior performance in recoupling half-integer-spin quadrupolar nuclei.

6. Materials and methods

6.1. Sample

m-Al_2O_3 was synthesized by Jean-Phillipe Dacquin at UCCS, Université de Lille [45]. The sample was used as received.

6.2. Simulations

Numerical simulations were performed using SPINEVOLUTION software [43], and assumed a static magnetic field of 9.4 T, except in Fig. S5, where B_0 = 18.8 T. The powder averaging was calculated using 144 pairs of $\{\alpha_{CR}, \beta_{CR}\}$ angles selected according to the method of Zaremba, Conroy, and Cheng [54–56] and 25 angles of γ_{CR}, which were equally stepped from 0 to 360°. The $\{\alpha_{CR}, \beta_{CR}, \gamma_{CR}\}$ Euler angles relate the crystal-fixed frame and the rotor-fixed one. For the ^{13}C-^{13}C spin system, the distance between two ^{13}C nuclei (r_{12}) was 1.54 Å, corresponding to $b_{12}/(2\pi)$ = −2.0 kHz, except in Fig. S7, where $b_{12}/(2\pi)$ = −0.28 kHz and in Figs. S9, S11, and S12, where $b_{12}/(2\pi)$ = −0.30 kHz. The ^{13}C offset is given in the figure captions. No ^{13}C CSA was included,

except in Figs. S7 and S9. For ^{13}C simulations, the MAS frequency was equal to ν_R = 66 kHz, except in Figs. S7, S9, S11, and S12, where ν_R = 13.889 kHz.

The ^{23}Na-^{23}Na spin system was defined as follows: r_{12} = 2.94 Å, corresponding to $b_{12}/(2\pi)$ = – 0.3 kHz. The Euler angles relating the internuclear ^{23}Na-^{23}Na vector to the crystal-fixed frame were equal to {0º, 0º, 0º}. Both ^{23}Na nuclei were subject to quadrupolar interactions with the following parameters: C_Q = 0 MHz and η_Q = 0 (Fig. S11) and C_Q = 1.0 MHz (Fig. S12a) or 10.0 MHz (Fig. S12b) and η_Q = 0.25. For an autocorrelation peak (Δ = 0 kHz), the isotropic chemical shifts for Na_1 and Na_2 nuclei are both 0 kHz.

The ^{27}Al-^{27}Al spin system was defined as follows: r_{12} = 3.0 Å, corresponding to $b_{12}/(2\pi)$ = – 0.3 kHz. The Euler angles relating the internuclear ^{27}Al-^{27}Al vector to the crystal-fixed frame were equal to {0º, 0º, 0º} unless stated otherwise. Both ^{27}Al nuclei were subject to quadrupolar interactions with the following parameters: C_Q = 3.0 MHz and η_Q = 0.25, except in Figs. S9-11, and S12b where C_Q = 0.1 or 1 kHz (Figs. S9-10) and 0 kHz (Fig. S11), both with η_Q = 0, and C_Q = 30.0 MHz with η_Q = 0.25 (Fig. S12b). The Euler angles describing the orientation of the ^{27}Al EFG tensor to the crystal-fixed frame were equal to {0º, 0º, 0º} for both ^{27}Al nuclei unless stated otherwise. For an autocorrelation peak (Δ = 0 kHz), the isotropic chemical shifts for Al_1 and Al_2 nuclei are both 0 kHz, whereas for a cross peak with Δ = 2.5 kHz, their isotropic chemical shifts are –1.25 and 1.25 kHz, respectively. No ^{27}Al CSA was included, and the MAS frequency was 13.889 kHz, except in Figs. S4 and S5.

We simulated the ^{13}C, ^{23}Na and ^{27}Al DQ-filtered 1D recoupling sequence given in Fig. 1d. For all simulations, the starting operator was I_{1z} or I_{2z} while the detecting operator was the raising operator associated to the CT $I_{jp}^{CT} = I_{jx}^{CT} + iI_{jy}^{CT}$ of the nucleus j = 1 or 2, except in Figs. S9-11, where the detecting operator was I_{2p} (= I_{2x} + iI_{2y}), or I_{1p}. The ^{23}Na-^{23}Na and ^{27}Al-^{27}Al DQ efficiencies were calculated by dividing the intensities of the DQ-filtered simulations by those of single-pulse simulations, in which the starting operator I_z is converted into the detecting operator I_p^{CT} by a ^{23}Na/^{27}Al CT-selective π/2 pulse, except in Figs. S9-11, where a non-selective π/2 pulse was used and the detecting operator was I_p. The amplitude of the RF-field during the recoupling

periods was equal to $\nu_R/2$ for ^{13}C, ^{23}Na, and ^{27}Al in the case of non-selective pulses (see Figs. S9-11), and $\nu_R/4$ for ^{23}Na and $\nu_R/6$ for ^{27}Al in the case of CT-selective pulses. Furthermore, the amplitude of $\pi/2$ and π pulses for ^{23}Na and ^{27}Al, which do not belong to the recoupling and last 8 and 16 µs, respectively, was equal to ν_{RF} = 31.2 kHz for non-selective excitation (see Figs. S9-11) and ν_{RF} = 15.6 kHz (^{23}Na) and 10.4 kHz (^{27}Al) for CT-selective excitation, respectively.

We also calculated the density matrix of a single ^{27}Al nucleus after the application of a single $BR2_2^1$, S_3 or [S_3] recoupling block (see Figs. 7, S13, and S14). The ^{27}Al nucleus was only subject to the isotropic chemical shift and the first-order quadrupolar interaction with C_Q = 3.0 MHz and η_Q = 0.25, except in Fig. S13, where C_Q = 0.1 and/or 1 kHz.

6.3. Experimental

All experiments were acquired on a 9.4 T widebore Bruker Biospin NMR magnet equipped with an AVANCE-II console and a 3.2 mm HXY MAS probe. At such magnetic field, the ^{27}Al Larmor frequency is 104.3 MHz. ν_R was set to 13.889 kHz. The ^{27}Al single-pulse MAS spectrum of Fig. 3a was acquired using a single CT-selective $\pi/2$ pulse whose amplitude and length were 10.4 kHz and 8 µs, respectively. 8 scans were accumulated and the recycling delay was 1.0 s. The ^{27}Al DQ-filtered 1D spectra were acquired using a sequence depicted in Fig. 1d with τ_{mix} = 1.73 ms for $BR2_2^1$ and τ_{mix} = 2.30 ms for [S_3]. During the recoupling, the RF amplitude was ~ 2.3 kHz, which corresponds to a CT nutation frequency equal to ~ 6.9 kHz. A CT-selective pulse with a flip angle of 3π was used to invert the ^{27}Al DQ coherences. The RF amplitude of other CT-selective $\pi/2$ and 3π pulses, lasting 8 and 46 µs, respectively, was ν_{RF} = 10.4 kHz. The recycling delay was 0.5 s and 128 scans were accumulated for both $BR2_2^1$ and [S_3] sequences.

Acknowledgements

We thank Dr. Jean-Philippe Dacquin and Dr. Aany Sofia Lilly Thankamony at UCCS for the synthesis of m-Al_2O_3 and the acquisition of the 2D ^{27}Al DQ-SQ correlation NMR spectrum, respectively. NTD thanks CEA and CNRS for his PhD grant. Chevreul Institute (FR 2638), Ministère de l'Enseignement Supérieur, de la Recherche et de l'Innovation, Hauts-de-France

Region and FEDER are acknowledged for supporting and funding partially this work. OL is also grateful for funding provided by ANR-18-CE08-0015-01 (ThinGlass) contract and Institut Universitaire de France. The NHMFL is funded by National Science Foundation (DMR-1644779) and the State of Florida. G.D.P. acknowledges the French National Research Agency (ANR-12-BS08-0016-01, ANR-11-LABX-0003-01 and RTB) and the European Research Council (ERC-CoG-2015, No. 682895), for financial support.

References

[1] E. R. R. Andrew, A. Bradbury, R. G. G. Eades, *Nature* **1958**, *182*, 1659–1659.

[2] S. Dusold, A. Sebald, in *Annual Reports on NMR Spectroscopy*, **2000**, pp. 185–264.

[3] R. Tycko, in *Encyclopedia of Magnetic Resonance*, John Wiley & Sons, Ltd, Chichester, UK, **2009**.

[4] C. P. Jaroniec, in *Encyclopedia of Magnetic Resonance*, John Wiley & Sons, Ltd, Chichester, UK, **2009**, pp. 189–212.

[5] G. De Paëpe, *Annual Review of Physical Chemistry* **2012**, *63*, 661–684.

[6] S. Paul, H. Takahashi, S. Hediger, G. De Paëpe, *Annual Reports on NMR Spectroscopy* **2015**, *85*, 93–142.

[7] A. P. M. Kentgens, *Geoderma* **1997**, *80*, 271–306.

[8] A. Jerschow, *Progress in Nuclear Magnetic Resonance Spectroscopy* **2005**, *46*, 63–78.

[9] S. E. Ashbrook, M. J. Duer, *Concepts in Magnetic Resonance Part A* **2006**, *28A*, 183–248.

[10] C. Fernandez, M. Pruski, in *Topics in Current Chemistry*, **2011**, pp. 119–188.

[11] P. P. Man, in *Encyclopedia of Magnetic Resonance*, John Wiley & Sons, Ltd, Chichester, UK, **2011**.

[12] P. Hartmann, C. Jäger, J. W. Zwanziger, *Solid State Nuclear Magnetic Resonance* **1999**, *13*, 245–254.

[13] T. G. Ajithkumar, A. P. M. Kentgens, *Journal of the American Chemical Society* **2003**, *125*, 2398–2399.

[14] T. G. Ajithkumar, E. R. H. Van Eck, A. P. M. Kentgens, *Solid State Nuclear Magnetic Resonance* **2004**, *26*, 180–186.

[15] M. Nijman, M. Ernst, A. P. M. Kentgens, B. H. Meier, *Molecular Physics* **2000**, *98*, 161–178.

[16] M. Baldus, D. Rovnyak, R. G. Griffin, *Journal of Chemical Physics* **2000**, *112*, 5902–5909.

[17] A. J. Painter, M. J. Duer, *The Journal of Chemical Physics* **2002**, *116*, 710–722.

[18] G. Mali, G. Fink, F. Taulelle, *The Journal of Chemical Physics* **2004**, *120*, 2835–2845.

[19] M. Edén, H. Annersten, Å. Zazzi, *Chemical Physics Letters* **2005**, *410*, 24–30.

[20] G. Mali, *Journal of magnetic resonance* **2007**, *185*, 318–25.

[21] A. J. Vega, *Journal of Magnetic Resonance (1969)* **1992**, *96*, 50–68.

[22] S. E. Ashbrook, S. Wimperis, *The Journal of Chemical Physics* **2004**, *120*, 2719–2731.

[23] S. E. Ashbrook, S. Wimperis, *The Journal of Chemical Physics* **2009**, *131*, 194509.

[24] N. C. Nielsen, H. Bildsøe, H. J. Jakobsen, M. H. Levitt, *The Journal of Chemical Physics* **1994**, *101*, 1805–1812.

[25] M. Edén, D. Zhou, J. Yu, *Chemical Physics Letters* **2006**, *431*, 397–403.

[26] A. Y. H. Lo, M. Edén, *Physical chemistry chemical physics : PCCP* **2008**, *10*, 6635–6644.

[27] M. Edén, A. Y. H. Lo, *Journal of Magnetic Resonance* **2009**, *200*, 267–279.

[28] M. Edén, *Solid state nuclear magnetic resonance* **2009**, *36*, 1–10.

[29] M. Edén, in *Modern Magnetic Resonance* (Ed.: G.A. Webb), Springer International Publishing, Cham, **2017**, pp. 1–33.

[30] M. Carravetta, M. Edén, X. Zhao, A. Brinkmann, M. H. Levitt, *Chemical Physics Letters* **2000**, *321*, 205–215.

[31] A. Brinkmann, M. H. Levitt, *Journal of Chemical Physics* **2001**, *115*, 357–384.

[32] M. H. Levitt, *eMagRes* **2007**, *9*, 165–196.

[33] B. Hu, Q. Wang, O. Lafon, J. Trébosc, F. Deng, J. P. Amoureux, *Journal of magnetic resonance* **2009**, *198*, 41–48.

[34] B. Hu, L. Delevoye, O. Lafon, J. Trébosc, J. P. Amoureux, *Journal of magnetic resonance* **2009**, *200*, 178–188.

[35] Q. Wang, B. Hu, F. Fayon, J. Trébosc, C. Legein, O. Lafon, F. Deng, J.-P. Amoureux, *Physical chemistry chemical physics : PCCP* **2009**, *11*, 10391–10395.

[36] Q. Wang, B. Hu, O. Lafon, J. Trébosc, F. Deng, J. P. Amoureux, *Journal of Magnetic Resonance* **2010**, *203*, 113–128.

[37] O. Lafon, J. Trébosc, B. Hu, G. De Paëpe, J.-P. Amoureux, *Chemical Communications* **2011**, *47*, 1–5.

[38] Q. Wang, B. Hu, O. Lafon, J. Trébosc, F. Deng, J. P. Amoureux, *Journal of Magnetic Resonance* **2009**, *200*, 251–260.

[39] D. Lee, H. Takahashi, A. S. L. Thankamony, J.-P. Dacquin, M. Bardet, O. Lafon, G. De Paëpe, *Journal of the American Chemical Society* **2012**, *134*, 18491–18494.

[40] G. Teymoori, B. Pahari, B. Stevensson, M. Edén, *Chemical Physics Letters* **2012**, *547*, 103–109.

[41] Y. Yu, P. Keil, M. R. Hansen, M. Edén, *Molecules* **2020**, *25*, 1–23.

[42] Y. Yu, P. Keil, B. Stevensson, M. R. Hansen, M. Edén, *Journal of Magnetic Resonance* **2020**, 106734.

[43] M. Veshtort, R. G. Griffin, *Journal of Magnetic Resonance* **2006**, *178*, 248–282.

[44] D. Lee, N. T. Duong, O. Lafon, G. De Paëpe, *The Journal of Physical Chemistry C* **2014**, *118*, 25065–25076.

[45] J. P. Dacquin, J. Dhainaut, D. Duprez, S. Royer, A. F. Lee, K. Wilson, *Journal of the American Chemical Society* **2009**, *131*, 12896–12897.

[46] U. Haeberlen, J. S. Waugh, *Physical Review* **1968**, *175*, 453–467.

[47] W. Magnus, *Commun. Pure Appl. Math.* **1954**, *7*, 649–673.

[48] MATLAB R2009a, The MathWorks Inc., Natick, Massachusetts, United States **2009**.

[49] A. J. Pell, K. J. Sanders, S. Wegner, G. Pintacuda, C. P. Grey, *Journal of Chemical Physics* **2017**, *146*, 194202.

[50] V. Vitzthum, M. A. Caporini, S. Ulzega, J. Trébosc, O. Lafon, J. P. Amoureux, G. Bodenhausen, *Journal of Magnetic Resonance* **2012**, *223*, 228–236.

[51] H. Colaux, D. M. Dawson, S. E. Ashbrook, *The Journal of Physical Chemistry A* **2014**, *118*, 6018–6025.
[52] A. Goldbourt, P. K. Madhu, S. Vega, *Chemical Physics Letters* **2000**, *320*, 448–456.
[53] P. K. Madhu, A. Goldbourt, L. Frydman, S. Vega, *Journal of Chemical Physics* **2000**, *112*, 2377–2391.
[54] S. K. Zaremba, *Annali di Matematica Pura ed Applicata, Series 4* **1966**, *73*, 293–317.
[55] H. Conroy, *The Journal of Chemical Physics* **1967**, *47*, 5307–5318.
[56] V. B. Cheng, H. H. Suzukawa, M. Wolfsberg, *Journal of Chemical Physics* **1973**, *59*, 3992–3999.